Materials Research Proceedings **27** (2023) 340-349 https://doi.org/10.21741/9781644902455-44

Numerical and experimental studies on the joint performance of fastened, bonded, and hybrid thin metal joints used in aircraft structures

Amir Ekladious[1, a *], John Wang[1, 2, b], Alan Baker[2, c], Nabil Chowdhury[1, d], Paul Chang[2, e], and Wing Kong Chiu[1, f]

[1]Department of Mechanical & Aerospace Engineering, Monash University, Clayton, VIC 3008, Australia

[2] Defence Science and Technology Group, 506 Lorimer Street, Fishermans Bend, VIC 3207, Australia

[a]amir.ekladious@monash.edu, [b]john.wang@defence.gov.au, [c]alanbaker@netspace.net.au, [d]nabil.chowdhury@monash.edu, [e]Paul.Chang1@defence.gov.au, [f]Wing.Kong.Chiu@monash.edu

Keywords: Adhesive Bonding and Mechanical Fastening Aluminium Joints, Finite Element Analysis (FEA), Static Strength

Abstract. Static strength of mechanically fastened, bonded, and hybrid double lap joints are investigated in this study. Aerospace grade 7075-T6 aluminium alloy was chosen for the adherend as it is a widely used primary aircraft structure material. Mechanical fasteners were arranged in square array patterns to resemble typical rivet arrangements in airframes. The aim was to compare the joint performance of three distinct joining/repairing mechanisms: purely riveted, purely bonded, and a hybrid of both rivets and adhesive bonding. Finite element analysis (FEA) verification of the riveted configuration static strength indicated accurate prediction of both joint strength and failure mode. Detailed results will be reported in the paper. This paper presents the first stage of a systematic research program assessing the damage tolerance behaviour of crack growth, and design assessment of adhesive bonded/hybrid metallic joints under static and fatigue loadings, to achieve the optimum joint design for applications.

Introduction

The exponential growth in air traffic calls for a reduction in airframe weight and increase in service life to address the concerns regarding fuel consumption and CO_2 emissions for environmental protection. Another major challenge is aircraft aging [1,2]. A study [3] on fuselage repairs of 71 Boeing 747 aircraft with an average lifespan of 29,500 flight hours, found that fatigue crack repairs constituted 58% of the total damage count (396 repairs), coming in second was corrosion damage (202 repairs, 29.4%), followed by impact damage (90 repairs, 13%). The increasing risk of fatigue related structural failure necessitates development and certification of advanced joining methods and tools.

Adhesive bonding has inherent mechanical advantages over mechanical fastening methods, such as pins, screws, bolts, and rivets, owing to: weight savings, sealing, elimination of galvanic corrosion, and relatively uniform stress distributions that avoid high stress concentrations otherwise present at fastener holes [5]. Repairs using adhesive bonding save millions of dollars and significantly enhance aircraft availability [6,7]. However, the challenge for adhesive bonding arises from certification requirements on some critical primary aircraft structures (e.g. a damaged single load-path primary structure with low residual strength) [7,8]. The main obstacles are: i) inability of current quality control procedures (for bonding operations undertaken in non-ideal situations) to demonstrate initial and ongoing bond integrity with sufficiently high probability of

Materials Research Proceedings **27** (2023) 340-349 https://doi.org/10.21741/9781644902455-44

reliability; and ii) current Non-destructive inspection (NDI) techniques are not yet available, or sufficiently reliable, to detect weak bonds in a practical situation. A promising approach that can address these concerns is the combination of both the mechanical and bonding techniques (i.e. hybrid joints).

A number of papers [9–14] investigating hybrid composite joints concluded that initial failure predominantly occurs due to disbonding. Therefore, mechanical fasteners can play an active role transferring load after bondline failure [9]. Hart-Smith's non-linear analysis of bonded and bolted joints [15] found that hybrid configurations could not significantly outperform adhesive bonding in intact, well-designed structures - though they might be able to stop the spread of defects or damage. Kelly [16] investigated the load distribution in single bolted hybrid joints (using FEA) concluding that the transfer is rather complicated owing to the differences in stiffness and alternate load paths. It was also found that bolt transfer load is directly proportional to both the adherend and adhesive thicknesses, and inversely proportional to overlap length, pitch distance, and adhesive modulus.

Methodology

Al 7075-T6 is characterised by high strength, toughness, good ductility, resistance to fatigue and extensively used in aircraft structures [17,18]. Table 1 summarises the relevant mechanical properties of the adherends.

Table 1: Mechanical properties of Al 7075-T6 at room temperature. [19,20]

$E\ (GPa)$	$\sigma_{yt}\ (MPa)$	$\sigma_{ut}\ (MPa)$	$\sigma_{yc}\ (MPa)$	$\%\delta$	ν
71.0	503	572	494.35	11	0.33

Cherry Maxibolt CR7621U-05-05 rivets are made of A286 Cres alloy, providing high strength, and excellent temperature and corrosion resistance; mechanical properties summarised in Table 2. During installation, the tail section of the rivet deforms into a flat circular "washer" to function as a large clamping region on the underside of the specimen.

Table 2: Mechanical properties of Cheri Maxibolt CR7621U rivet at room temperature. [21]

$E\ (GPa)$	$\sigma_{yt}\ (MPa)$	$\sigma_{ut}\ (MPa)$	$\%\delta$	ν
201.0	655	965	12	0.3

FM73 film adhesive manufactured by Cytec Engineered Materials [22] is an aerospace grade adhesive which provides excellent peel strength, good moisture and corrosion resistance in high humidity environments. The manufacturer's recommended cure condition is 45psi at $120°C$ for 1 hour.

The riveted joints were designed in accordance with the Federal Aviation Administration (FAA) regulations [23]. For protruding head rivets, the FAA standards establish a minimum allowable edge distance of 2 rivet diameters, and rivet pitch of 4 rivet diameters. Specimen rivet spacings were set $1/16''$ (1.6 mm) larger than the recommended minimum to preserve minimum spacing limits due to variations in rivet diameters. For a bonded joint the outer adherend commonly has a 1:10 linear taper at the end with half the edge thickness of the outer adherend to reduce the adhesive peak stress [24–26], which would result in a tapered region of 8 mm in length at both ends. However, this was omitted in the current specimen configurations, not only for simplification but also for the consideration that a possible disbond defect could render the taper ineffective, whilst this research is focused on damage tolerance assessment.

Fig. 1 shows a schematic of the fastened/hybrid configuration of the double lap joint. The bonded specimen has the same adherend dimensions with the omission of fasteners.

Materials Research Proceedings **27** (2023) 340-349 https://doi.org/10.21741/9781644902455-44

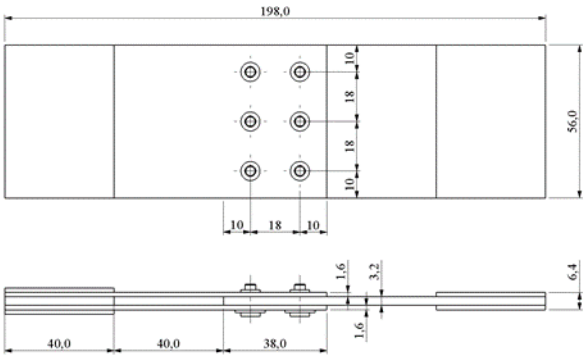

Figure 1: Double lap joint configuration containing six fasteners in a square array (dimensions in mm).

Fastener holes in aircraft assemblies are critical regions from where fatigue damage can initiate in metallic parts. Manufacturers, like Airbus, observed that hole machining processes such as drilling, reaming, and cold expansion could significantly increase the fatigue strength [27]. Cold expansion during riveting [28–31] greatly improves fatigue life of aluminium alloy joints by introducing compressive residual stress at the hole. Subsequently, the service life of holed parts increases significantly since it is difficult for cracks to propagate through a compressive field [6,32]. To capture this effect, riveted and hybrid configurations were drilled and reamed using a 4.20 mm reamer, producing a 0.02 mm clearance to allow for cold working under the forces of expanding rivets.

A standard surface treatment [33–35] used by Defence Science and Technology Group (DST Group) was applied. It includes solvent degreasing using Methyl-Ethyl-Ketone (MEK) and residue removal using distilled water prior to surface roughening by aluminium oxide grit blasting. The final step is an organosilane coupling agent applied to improve the hydrolytic resistance of adhesive bonds formed between metal and epoxy adhesive. The Boeing Wedge Test (BWT) ASTM D3762 [36], widely-used for quality control and validating bonding processes in aircraft joints, was employed to verify bond quality.

Aluminium adherends were machined and assembled into their fastened, bonded, and hybrid configurations. Specimens requiring film adhesive and rivets were co-cured in an autoclave. Autoclaves apply positive pressure to the adhesive, such that gaps between rivets and fastener holes became filled with adhesive.

The non-linear implicit solver of Abaqus 2021 [37] was used to model the loading behaviour of the fastened joint and validated against the experimental data. The adherends were modelled using the isotropic material properties defined in Table 1. The rivets were modelled using elastic-plastic material data specified in Table 2. In order for the FE model to capture the global and local behaviour of the joints efficiently and the stress state in their critical locations, finer geometrical details and meshing in the critical regions, the material behaviour, rivet pre-tensioning, type of fastener fit, friction, load distribution, as well as contact interactions between the surfaces were included in the numerical model [38–41]. The washer, rivet/bolt, and nut were modelled as one part as in [38] to simplify the model and reduce the required computing resources by decreasing the number of elements and contact bodies.

The FE mesh was constructed using 3D continuum hexahedral linear elements, as quadratic elements suffer from inaccuracy in contact modelling [37]. However, under bending, the edges of linear elements cannot describe the curvature accurately, which can cause artificial shear stresses via shear locking [37]. Shear locking can cause the model to be overly stiff as observed by Ireman [38]. To solve this, the incompatible mode elements (C3D8I) in Abaqus were used to add degrees of freedom to improve the bending behaviour of fully integrated linear elements. Linear elements with reduced order of integration (C3D8R) could also be used to combat over-stiffness [42] but they suffer from hourglassing which can lead to severe mesh distortion in joint models [43]. To

Materials Research Proceedings **27** (2023) 340-349 https://doi.org/10.21741/9781644902455-44

reduce the computational time, C3D8I elements were used in regions where high stress gradients were expected to occur, and the less expensive C3D8R elements elsewhere.

Several grids were constructed and tested. The final meshes were generated conforming to the meshing strategy used in [39,40] as they were found to significantly reduce the calculation time with negligible effects on the results when compared to finer meshes. To achieve this, the overlapping joint regions were heavily partitioned to allow for dense structured meshing in the areas of high stress gradients and coarser meshes elsewhere as shown in Fig. 2a. Tie constraints were applied to join the joint gauge region and the rest of the laminates together. The resultant grid is shown in Fig. 2b. The seed element size was increased from 0.2 to 0.6 in the high gradient regions. The average element aspect ratio was maintained to be less than 5 in all cases.

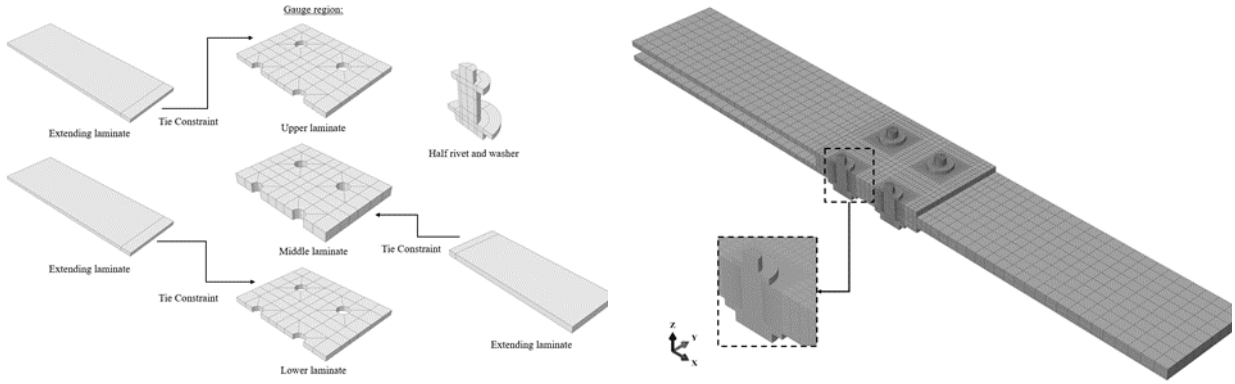

(a) (b)

Figure 2: The double lap joint assemblies showing the (a) partitioning strategy, and (b) mesh.

To represent the tensile experimental setup, a clamped boundary condition ($u_x = u_y = u_z = 0$), and a displacement vector in solely the axial direction were applied on the left and right ends, respectively. A symmetry condition was also applied to the plane midway through the joint width to reduce the model size and computational time.

Contact conditions were set by defining contact pairs between interacting surfaces. By definition, slave surfaces are not allowed to penetrate their corresponding master surface. As a rule of thumb, master roles should be assigned to surfaces of stiffer bodies which were given coarser meshes. The surface-to-surface discretisation technique was used, as it prevented surface penetration in an average sense and generally provides more accurate results than node-to-surface discretisation [37]. The node-to-surface method can also lead to a flawed radial strain field [40]. In order to avoid the creation of discontinuous surface normals due to the abrupt changes in the joint geometries, the surfaces were broken down into several contact pairs as in [39]. The finite sliding formulation is then selected to allow for arbitrary travel of contacting surfaces. The tangential behaviour of the surface pairs was modelled using the penalty friction formulation, and the friction coefficients between the adherends, and the adherends and fastener were based on [44]. The hard contact method, which attempts to strictly enforce a pressure-overclosure relationship [37], was specified to enforce normal contact.

The main issue to obtain convergence was the phenomenon known as contact chattering, where the status of some of the slave nodes changes repeatedly between open and closed when an initial overlap or penetration of the discretised contact surfaces occur [37]. This leads to severe discontinuity iterations (SDIs) which can result in failure to convergence. To aid the solver in reaching a solution to account for the residual stresses induced by the cold expansion of the fastener hole during the riveting process that results in an interference fit as previously discussed, the overlap was resolved in a manner where there are stresses and strains when moving the nodes to a non-overlapping position. In this case, the solver was instructed to treat the overclosure as an

interference fit in a separate step by gradually removing the slave node overclosure then automatically shrink fit the deformed slave nodes to adjust the overclosure [37]. Further improvements in contact convergence were obtained by using the unsymmetric solver, recommended due to the high curvature of the master surfaces [37] and contact stabilisation. The amount of contact stabilisation was chosen such that the energy dissipated by viscous damping was negligible.

The static experimental testing in this study focused primarily on tensile response of the double lap joints to determine the load-displacement characteristics of each configuration type. For this discussion, specimens are considered to have three regions. The first is the *joined region* and it is the central area of interest where the joint is assembled. The second is the *remote region*, the visible part of the adherends between the joined region and where the specimen is clamped. Finally, the end of the test specimen clamped by the machine is known as the *end region*. Two strain gauges were used at the joined and remote regions, respectively, as shown in Fig.3.

The recorded total displacement by the testing machine comprises the deformation of the load train in addition to that of the test specimen. To determine the true displacement of the specimen from the machine transducer, the load train needs to be isolated [45]. A calibrated extensometer was used on a rectangular coupon specimen with the thickness of the central adherend and same dimensions and material as the double lap joint to determine the load train's compliance. Then, the calibration factor between the cross-head displacement and the true displacement between sample's ends can be calculated accordingly as illustrated in Fig. 4.

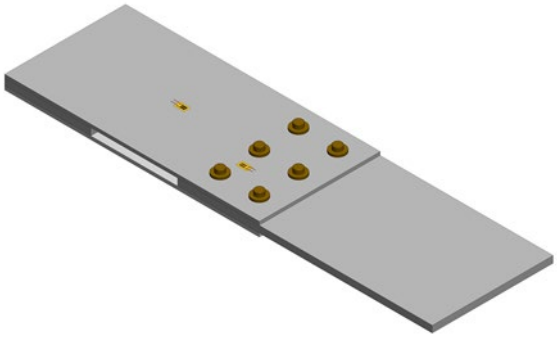

Figure 3: The strain gauges location on the samples. (The same location is used on all configurations)

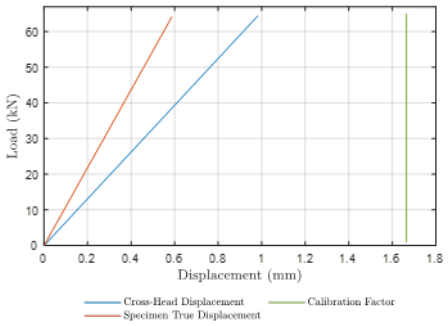

Figure 4: Determining the calibration factor for the specimens' true displacement.

Results and Discussion

Trial analyses were carried out to investigate the effects of different interference fit values between the rivet and hole on the induced residual stress. An interference value of $35\mu m$ was then assumed, as the maximum induced stress was in the limit range of the yielding stress of the adherends as shown in Fig. 5.

Figure 5: Induced residual stresses due to cold expansion of the rivet hole by an interference value of $35\mu m$ *during the riveting process.*

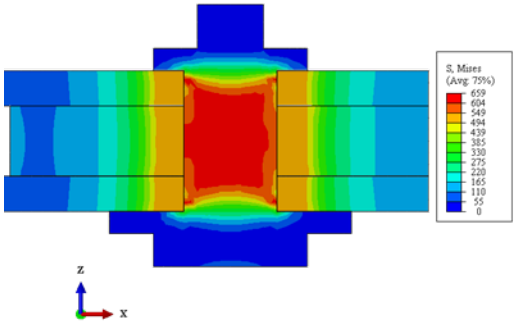

Materials Research Proceedings **27** (2023) 340-349 https://doi.org/10.21741/9781644902455-44

The calibrated experimental load-displacement comparison of the three configuration types is shown in Fig. 6. The riveted configuration had the lowest loading capability and stiffness out of the three types due to the aforementioned reasons. The bonded and hybrid joints had the same stiffness, however the bonded configuration was able to withstand slightly higher load before failure. The hybrid configuration failed at the holes while the riveted joint through bearing failure due to stress concentrations around the hole. However, in case of the bonded joint, the specimen failed outside of the joined region by tension failure of the adherend section, leaving the bondline intact. Fracture images of the three configurations are shown in Fig. 7. The FEA prediction of riveted joint behaviour is shown in Fig. 6. The model showed good agreement with the experimental data and accurately predicted the failure mode.

The load-strain comparison for each joint type at their joined and remote regions is shown in Fig. 8a. The joined region strain for the bonded and hybrid joints were much stiffer than the riveted type, and therefore the outer adherends experienced higher strain till failure. Strain gauges installed at the remote region of bonded and hybrid joints were overloaded at $\sim 16400 \mu\varepsilon$, corroborating adherend failure. The strain behaviour of the hybrid configuration at the joined region before failure in Fig. 8b, shares similar behaviour to the bonded response, followed by a modest load increase that tapers down toward failure. This indicated that the bonded region of the joint (behind the rivet row) withstanding load up to $\sim 96 kN$ at a strain of $\sim 4400 \mu\varepsilon$ before it failed, and passed the load to the rivets row, where the disbond occurred. Eventually, the outer adherend reached a maximum strain of $\sim 4575 \mu\varepsilon$ before the middle adherend started yielding and finally failed at the rivet holes.

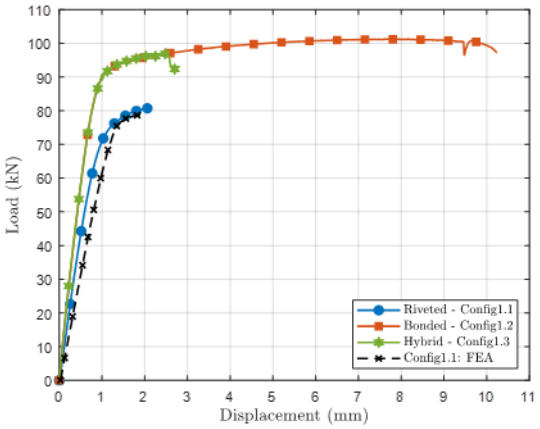

Figure 6: Calibrated experimental load-displacement comparison for the three joint types and FEA for the riveted configuration.

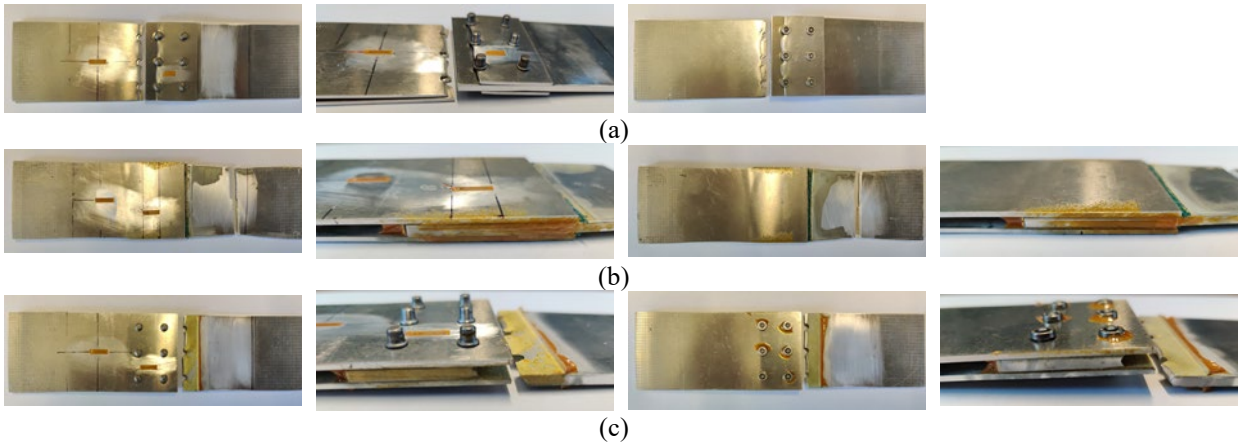

Figure 7: Failure behaviour for the (a) riveted, (b) bonded, and (c) hybrid configurations.

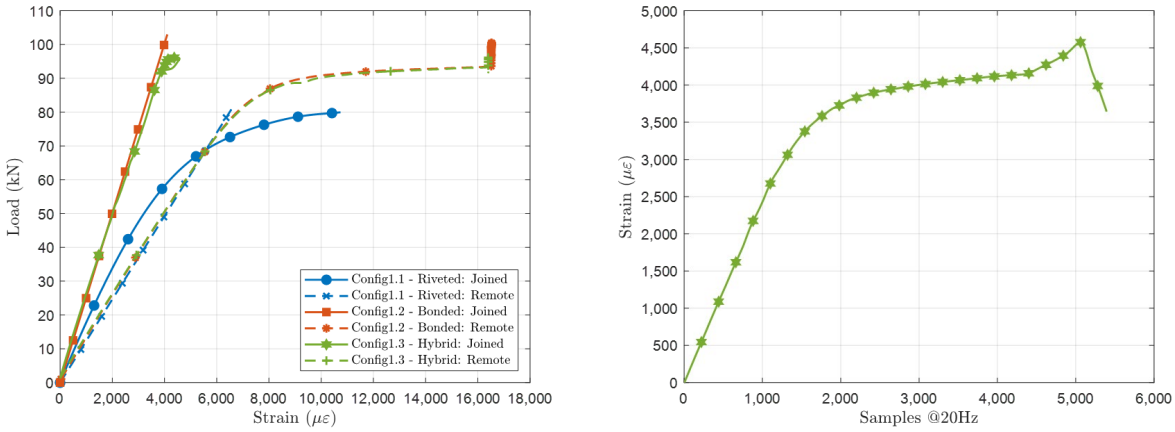

(a) (b)

Figure 8: (a) Load vs strain comparison for the three joint types on the Joined & Remote Regions. (b) The joined region strain behaviour for the hybrid configuration.

Conclusion and future work

The static loading behaviour of riveted, bonded, and hybrid double lap joint configurations has been compared experimentally. The mechanically fastened configuration had the lowest stiffness and loading capacity. Bonded and hybrid joints on the other hand showed similar joint stiffness. The bonded configuration was able to hold slightly higher load than the hybrid counterpart due to the lack of fastener holes which decrease the effective bonding area and introduce stress concentrations in their vicinity. However, the addition of rivets to a bonded configuration has the benefit of safeguarding the joint in case of disbonding or the presence of defects within the bondline. This could help in certifying these joining/patching techniques for use on primary aircraft structures. FEA was able to accurately predict the loading behaviour and failure mode of the riveted configuration and matched the experimental data well. Comparison of strain behaviour for all three joint configurations at the joined and remote regions provides understanding of the failure mechanisms, noting details such as load transfer from bondline failure to adjacent rivets in hybrid joints. For future work, more static tests are planned to ensure the results are statistically sound, followed by a comparison of fatigue behaviour between the three joint types with the inclusion of adhesive defects to simulate quality issues or environmental effects that could happen in practice and their effect on performance. FEM modelling will be extended to include bonded and hybrid joints.

Funding
This research is partially funded by the Australian Defence Science and Technology Group. The financial and training support by DST Group is gratefully acknowledged.

References

[1] Horst P, Trey H. Structural maintenance of ageing aircraft: SMAAC. Air Sp Eur 1999;1:71–4. https://doi.org/10.1016/s1290-0958(00)88875-9.

[2] Goranson UG. Fatigue issues in aircraft maintenance and repairs. Int J Fatigue 1998;20:413–31. https://doi.org/10.1016/S0142-1123(97)00029-7.

[3] Vogelesang LB, Vlot A. Development of fibre metal laminates for advanced aerospace structures. J Mater Process Technol 2000;103:1–5. https://doi.org/10.1016/S0924-0136(00)00411-8.

[4] Okafor AC, Bhogapurapu H. Design and analysis of adhesively bonded thick composite patch repair of corrosion grind-out and cracks on 2024 T3 clad aluminum aging aircraft structures. Compos Struct 2006;76:138–50. https://doi.org/10.1016/j.compstruct.2006.06.020.

[5] Adams RD, Comyn J, Wake WC. Structural Adhesive Joints in Engineering 2/e. Assem Autom 2000;20:136–40. https://doi.org/10.1108/aa.2000.03320bae.002.

[6] Wang J, Baker A, Chang P. Hybrid approaches for aircraft primary structure repairs. Compos Struct 2019;207:190–203. https://doi.org/10.1016/j.compstruct.2018.09.038.

[7] Baker AA, Wang J. Chapter 6 adhesively bonded repair/reinforcement of metallic airframe components. Mater. Process. Des. Propos. through-life Manag. Aircr. Sustain. repair, 2017.

[8] Baker A, Gunnion A, Wang J. On the certification of bonded repairs to primary composite aircraft components. J Adhes 2015;91:4–38. https://doi.org/10.1080/00218464.2014.883315.

[9] Hart-Smith LJ. Bonded-bolted composite joints. J Aircr 1985;22:993–1000. https://doi.org/10.2514/3.45237.

[10] Kweon JH, Jung JW, Kim TH, Choi JH, Kim DH. Failure of carbon composite-to-aluminum joints with combined mechanical fastening and adhesive bonding. Compos Struct 2006;75:192–8. https://doi.org/10.1016/j.compstruct.2006.04.013.

[11] Barut A, Madenci E. Analysis of bolted-bonded composite single-lap joints under combined in-plane and transverse loading. Compos Struct 2009;88:579–94. https://doi.org/10.1016/j.compstruct.2008.06.003.

[12] Matsuzaki R, Shibata M, Todoroki A. Improving performance of GFRP/aluminum single lap joints using bolted/co-cured hybrid method. Compos Part A Appl Sci Manuf 2008;39:154–63. https://doi.org/10.1016/j.compositesa.2007.11.009.

[13] Chowdhury NM, Wang J, Chiu WK, Chang P, Kong Chiu W, Chang P. Experimental and finite element studies of thin bonded and hybrid carbon fibre double lap joints used in aircraft structures. Compos Part B Eng 2015;85:233–42. https://doi.org/10.1016/j.compositesb.2015.09.038.

[14] Chowdhury N, Chiu WK, Wang J, Chang P. Static and fatigue testing thin riveted, bonded and hybrid carbon fiber double lap joints used in aircraft structures. Compos Struct 2015;121:315–23. https://doi.org/10.1016/j.compstruct.2014.11.004.

[15] Hart-Smith LJ. Bolted and Bonded Joints. vol. 21. ASM International; 2001. https://doi.org/10.31399/asm.hb.v21.a0003384.

[16] Kelly G. Load transfer in hybrid (bonded/bolted) composite single-lap joints. Compos Struct 2005;69:35–43. https://doi.org/10.1016/j.compstruct.2004.04.016.

[17] ASM International Handbook Committee. ASM handbook Volume 2 - Properties and selection: Nonferrous alloys and special-purpose materials. ASM Met Handb 1993;2:137.

[18] Crawford BR, Loader C, Harrison TJ, Liu Q. A Demonstration using Low-k t Fatigue Specimens of a Method for Predicting the Fatigue Behaviour of Corroded Aircraft Components 2013.

[19] Anderson K, Weritz J, Kaufman JG. ASM Handbook®, Volume 2B - Properties and Selection of Aluminum Alloys. vol. 2. ASM International; 2019. https://doi.org/10.31399/asm.hb.v02b.a0006737.

[20] Mathauser EE. Compressive Stress-Strain Properties of 7075-T6 Aluminum-Alloy Sheet at Elevated Temperatures. Washington, D.C.: National Advisory Committee for Aeronautics; 1956.

[21] Cherry Maxibolt blind bolt. California: Cherry Aerospace; 2007.

[22] Cytec. Fm 73 Epoxy Film Adhesive Technical Data Sheet. Cytec Engineered Materials; 2011.

[23] United States. Flight Standards Service. Aviation Maintenance Technician Handbook - Airframe: FAA-H-8083-31. vol. 1. 2018.

[24] Andreassi L, Baudille R, Biancolini ME. Spew formation in a single lap joint. Int J Adhes Adhes 2007;27:458–68. https://doi.org/10.1016/j.ijadhadh.2006.07.002.

[25] Belingardi G, Goglio L, Tarditi A. Investigating the effect of spew and chamfer size on the stresses in metal/plastics adhesive joints. Int J Adhes Adhes 2002;22:273–82. https://doi.org/10.1016/S0143-7496(02)00004-0.

[26] Wang J, Rider AN, Heller M, Kaye R. Theoretical and experimental research into optimal edge taper of bonded repair patches subject to fatigue loadings. Int J Adhes Adhes 2005;25:410–26. https://doi.org/10.1016/j.ijadhadh.2004.11.007.

[27] Lacombe A, Landon Y, Paredes M, Chirol C, Benaben A. Numerical evaluation of residual stress induced by reaming of aluminium 2024-T351. Int. Jt. Conf. Mech. Des. Eng. Adv. Manuf., Cartagena, Spain: 2018. https://doi.org/hal-02127580.

[28] Özdemir AT, Hermann R. Effect of expansion technique and plate thickness on near-hole residual stresses and fatigue life of cold expanded holes. J Mater Sci 1999;34:1243–52. https://doi.org/10.1023/A:1004521309415.

[29] Lacarac V, Smith DJ, Pavier MJ, Priest M. Fatigue crack growth from plain and cold expanded holes in aluminum alloys. Int J Fatigue 2000;22:189–203. https://doi.org/10.1016/S0142-1123(99)00126-7.

[30] Chakherlou TN, Vogwell J. The effect of cold expansion on improving the fatigue life of fastener holes. Eng Fail Anal 2003;10:13–24. https://doi.org/10.1016/S1350-6307(02)00028-6.

[31] Newman JC, W. Steven Johnson J, Zhao W. Assessment of Residual Stresses and Hole Quality on the Fatigue Behavior of Aircraft Structural Joints Volume 1 : Stress Analyses ,

Fatigue Tests , and Life Predictions. Washington DC: 2009. https://doi.org/DOT/FAA/AR-07/56,V1.

[32] Lai MO, Oh JT, Nee AYC. Fatigue properties of holes with residual stresses. Eng Fract Mech 1993;45:551–7. https://doi.org/10.1016/0013-7944(93)90262-Q.

[33] Davis MJ. Bonded Repairs: Principles and Practice 1991.

[34] Davis M, Bond D. Principles and practices of adhesive bonded structural joints and repairs. Int J Adhes Adhes 1999;19:91–105. https://doi.org/10.1016/S0143-7496(98)00026-8.

[35] Rider AN. Prebond Inspection Techniques to Improve the Quality of Adhesive Bonding Surface Treatments. 2006.

[36] ASTM D3762 - Standard Test Method for Adhesive-Bonded Surface Durability of Aluminum (Wedge Test) n.d.

[37] Smith M. ABAQUS/Standard User's Manual, Version 6.9. Providence, RI, USA: Dassault Systèmes Simulia Corp; 2009.

[38] Ireman T. Three-dimensional stress analysis of bolted single-lap composite joints. Compos Struct 1998;43:195–216. https://doi.org/10.1016/S0263-8223(98)00103-2.

[39] Egan B, McCarthy CT, McCarthy MA, Frizzell RM. Stress analysis of single-bolt, single-lap, countersunk composite joints with variable bolt-hole clearance. Compos Struct 2012;94:1038–51. https://doi.org/10.1016/j.compstruct.2011.10.004.

[40] McCarthy MA, McCarthy CT, Lawlor VP, Stanley WF. Three-dimensional finite element analysis of single-bolt, single-lap composite bolted joints: Part I - Model development and validation. Compos Struct 2005;71:140–58. https://doi.org/10.1016/j.compstruct.2004.09.024.

[41] Stocchi C, Robinson P, Pinho ST. A detailed finite element investigation of composite bolted joints with countersunk fasteners. Compos Part A Appl Sci Manuf 2013;52:143–50. https://doi.org/10.1016/j.compositesa.2012.09.013.

[42] Camanho PP, Matthews FL. Delamination onset prediction in mechanically fastened joints in composite laminates. J Compos Mater 1999;33:906–27. https://doi.org/10.1177/002199839903301002.

[43] Hühne C, Zerbst AK, Kuhlmann G, Steenbock C, Rolfes R. Progressive damage analysis of composite bolted joints with liquid shim layers using constant and continuous degradation models. Compos Struct 2010;92:189–200. https://doi.org/10.1016/j.compstruct.2009.05.011.

[44] FULLER DD. Coefficients of Friction. In: Gray DE, editor. Am. Inst. Phys. Handb. 3rd ed., McGraw-Hill Book Company; 1973. https://doi.org/10.1088/0031-9112/24/8/017.

[45] Chalkley PD, Chiu WK. An improved method for testing the shear stress/strain behaviour of adhesives. Int J Adhes Adhes 1993;13:237–42. https://doi.org/10.1016/0143-7496(93)90026-6.